crystals

MDPI

Article

Solvothermal Synthesis of Calcium Hydroxyapatite via Hydrolysis of Alpha-Tricalcium Phosphate in the Presence of Different Organic Additives

Rasa Karalkeviciene [1], Eva Raudonyte-Svirbutaviciene [1], Aleksej Zarkov [1,*], Jen-Chang Yang [2], Anatoli I. Popov [3] and Aivaras Kareiva [1]

[1] Institute of Chemistry, Faculty of Chemistry and Geosciences, Vilnius University, Naugarduko 24, LT-03225 Vilnius, Lithuania
[2] Graduate Institute of Nanomedicine and Medical Engineering, College of Biomedical Engineering, Taipei Medical University, 250 Wu-Hsing St., Taipei 11052, Taiwan
[3] Institute of Solid State Physics, University of Latvia, Kengaraga 8, LV-1063 Riga, Latvia
* Correspondence: aleksej.zarkov@chf.vu.lt

Abstract: In this study, the effects of sodium lauryl sulfate and various amino acids (DL-aspartic acid, dodecanedioic acid, and suberic acid) on the formation of calcium-deficient hydroxyapatite via hydrolysis of α-tricalcium phosphate (α-TCP) were investigated; moreover, a combined effect of these additives and ethylene glycol as a synthesis medium was also estimated. The hydrolysis reaction was performed in solutions containing different concentrations of additives in aqueous and mixed aqueous–organic media under solvothermal conditions. It was demonstrated that the nature and the concentration of organic additives influence the phase purity and morphology of the final product. Higher concentrations of sodium lauryl sulfate and dodecanedioic acid induced the formation of impurities in addition to hydroxyapatite, while aspartic and suberic acid did not affect the phase purity. The morphology of the samples varied from plate- to rod-like depending on the concentrations of specific organic additive.

Keywords: calcium hydroxyapatite; α-tricalcium phosphate; amino acids; organic additives; solvothermal synthesis

Citation: Karalkeviciene, R.; Raudonyte-Svirbutaviciene, E.; Zarkov, A.; Yang, J.-C.; Popov, A.I.; Kareiva, A. Solvothermal Synthesis of Calcium Hydroxyapatite via Hydrolysis of Alpha-Tricalcium Phosphate in the Presence of Different Organic Additives. *Crystals* **2023**, *13*, 265. https://doi.org/10.3390/cryst13020265

Academic Editor: Ruikang Tang

Received: 5 January 2023
Revised: 30 January 2023
Accepted: 1 February 2023
Published: 3 February 2023

1. Introduction

Calcium phosphates (CPs) are the group of materials which are widely used in different areas, including medicine and bone regeneration [1], catalysis [2], sorption of organic pollutants [3], and heavy metals [4], as host matrices for the development of optical materials [5] and many others. Probably, the most popular member of the CPs family is calcium hydroxyapatite ($Ca_{10}(PO_4)_6(OH)_2$, HAp), which is the main inorganic component of human hard tissues.

HAp crystallizes in a hexagonal crystal structure with a space group $P6_3/m$. The crystal structure of HAp is notable due to the fact that it has two types of crystal planes, namely, *a*-face and *c*-face. The *a*-face is positively charged due to calcium ions, while the *c*-face is negatively charged due to oxygen atoms belonging to phosphate ions [6]. Anisotropic growth of HAp crystals in one or another crystallographic direction is an important factor from the point of view of specific interaction of oriented crystals with other substances, which may lead to enhanced performance and specific application of this material. For example, the adsorption of proteins on HAp crystals depends on their morphology. Different types of proteins, such as basic and acidic proteins, can adsorb selectively on the crystal planes of HAp [7,8]. Another effect of crystallographically oriented HAp particles was shown by Goto et al. [3] who demonstrated that tuning the morphology of HAp crystals may lead to enhanced or selective adsorption of cationic or anionic dyes. In this light,

the controllable synthesis of plate-like or rod-like crystals with different aspect ratios and surface charges is an important task for many industries and purification technologies.

Synthetic HAp can be obtained in a variety of ways, including solid-state reaction [9], sol-gel method [10], as well as wet precipitation [11], hydrothermal [12] and solvothermal syntheses [13], and others. Another group of synthetic approaches employed for the synthesis of HAp considers the phase conversion from other less stable CPs. For instance, Ca-deficient HAp can be obtained through the transformation from alpha-tricalcium phosphate ($Ca_3(PO_4)_2$, α-TCP) or amorphous CP in aqueous medium [14]. Synthetic pathways employing high-temperature treatment, such as solid-state reaction or sol-gel, usually result in the formation of large agglomerated particles and do not lead to the anisotropic growth of the crystals. Crystallographically oriented products are usually obtained by low-temperature wet chemical methods.

Functional groups of organic substances, such as carboxyl or amino, can specifically interact with the planes of HAp particles during the crystal growth process and affect particle growth in one or another direction. Different additives were previously employed in order to investigate their effect on the crystal growth, morphology, and properties of HAp. For instance, Suchanek et al. [15] successfully synthesized HAp nanofibers in the presence of monoethanolamine under hydrothermal conditions. In et al. [16] investigated the role of sebacic acid on the formation of HAp and demonstrated that sebacic acid can accelerate nucleation and act as an inhibitor in the specific direction of HAp crystal growth. Jiang et al. [17] showed that poly(acrylic acid), depending on its concentration, can promote or inhibit HAp crystallization; moreover, the composition of mixed aqueous–organic reaction medium also has an effect on the crystallization and morphology of HAp [18].

In the present work, a comprehensive study has been performed to investigate the influence of various organic additives on the phase purity and morphology of HAp synthesized via a hydrolysis of α-TCP under hydrothermal/solvothermal conditions. The effects of different concentrations of sodium lauryl sulfate (SLS, $CH_3(CH_2)_{11}OSO_3Na$) and three amino acids—dodecanedioic acid ($C_{12}H_{22}O_4$), DL-aspartic acid ($C_4H_7NO_4$), and suberic acid ($C_8H_{14}O_4$)—were studied and compared. To the best of our knowledge, the effect of these additives on the hydrolysis of low-temperature synthesized metastable α-TCP and simultaneous formation of HAp had never been investigated. These compounds have different functional groups and different carbon chain length. Two of the selected molecules contain only carboxyl groups (dodecanedioic and suberic acids); however, they have different chains containing 12 and 8 carbon atoms, respectively. Aspartic acid has a very short chain having only 4 carbon atoms. At the same time, in addition to the carboxyl group, there is a $–NH_2$ group in this molecule. Finally, sodium lauryl sulfate has a long chain (C12) and an SO_4^- functional group, which is absent in other selected molecules; moreover, a complex effect of amino acids and ethylene glycol was studied as well.

2. Materials and Methods

2.1. Synthesis

Starting α-TCP powders were synthesized following the procedure described elsewhere [19]. Briefly, a certain amount (3.42 g) of calcium nitrate tetrahydrate ($Ca(NO_3)_2{\cdot}4H_2O$, 99%, Roth, Karlsruhe, Germany) was dissolved in 20 mL of deionized water and a portion of diammonium hydrogen phosphate ($(NH_4)_2HPO_4$, 98%, Roth, Karlsruhe, Germany) (1.27 g) was dissolved in a separate beaker in 15 mL of deionized water. After a full dissolution, 5 mL of concentrated ammonium hydroxide (NH_4OH, 25%, Roth, Karlsruhe, Germany) was added to the $(NH_4)_2HPO_4$ solution and stirred; subsequently, the Ca-containing solution was added, rapidly resulting in the formation of white precipitates, which were aged in the solution for 10 min. Next, the precipitates were filtered and washed with 100 mL of deionized water and 150 mL of isopropyl alcohol. The synthesis product was dried overnight in an oven at 50 °C and annealed at 700 °C for 5 h with a heating rate of 5 °C/min.

The α-TCP was further used as a precursor for the synthesis of hydroxyapatite (HAp) via a hydrolysis reaction under hydrothermal conditions. The reactions were performed in the presence of different concentrations of sodium lauryl sulfate (SLS, $NaC_{12}H_{25}SO_4$, ≥99%, Roth, Karlsruhe, Germany) and amino acids—dodecanedioic acid (DDDA, $C_{12}H_{22}O_4$, 99%, Sigma Aldrich, Darmstadt, Germany), DL-aspartic acid (Asp, $C_4H_7NO_4$, 99%, Sigma Aldrich, Darmstadt, Germany), and suberic acid (Sa, $C_8H_{14}O_4$, 99%, Sigma Aldrich, Darmstadt, Germany). In a typical procedure, 0.3 g of α-TCP powder and appropriate amount of SLS or amino acids were placed into a 90 mL polytetrafluoroethylene-lined stainless-steel pressure vessel, diluted with 20 mL of water, and treated at 200 °C for 5 h.

Solvothermal reactions were performed in the presence of different concentrations of DL-aspartic acid and suberic acid in water and ethylene glycol (W:EG) mixture (v/v ratio of 40:60). The synthetic procedure was analogical to that with aqueous solutions.

After the hydrothermal treatment the resulting powders were filtered, washed with ethyl alcohol, and dried at 50 °C overnight. The sample notations and concentrations of additives in the reaction solution are given in Table 1.

Table 1. Sample codes, used organic additive, concentration of additives, and reaction media.

Notation	Organic Additive	Concentration of Additive	Water to Ethylene Glycol Ratio (v/v)
SLS:005	Sodium lauryl sulfate	0.005 mol/L	100:0
SLS:025	Sodium lauryl sulfate	0.025 mol/L	100:0
SLS:05	Sodium lauryl sulfate	0.05 mol/L	100:0
SLS:075	Sodium lauryl sulfate	0.075 mol/L	100:0
SLS:1	Sodium lauryl sulfate	0.1 mol/L	100:0
DDDA:005	Dodecanedioic acid	0.005 mol/L	100:0
DDDA:025	Dodecanedioic acid	0.025 mol/L	100:0
DDDA:05	Dodecanedioic acid	0.05 mol/L	100:0
DDDA:075	Dodecanedioic acid	0.075 mol/L	100:0
DDDA:1	Dodecanedioic acid	0.1 mol/L	100:0
Asp:005	DL-Aspartic acid	0.005 mol/L	100:0
Asp:025	DL-Aspartic acid	0.025 mol/L	100:0
Asp:05	DL-Aspartic acid	0.05 mol/L	100:0
Asp:075	DL-Aspartic acid	0.075 mol/L	100:0
Asp:1	DL-Aspartic acid	0.1 mol/L	100:0
Sa:005	Suberic acid	0.005 mol/L	100:0
Sa:025	Suberic acid	0.025 mol/L	100:0
Sa:05	Suberic acid	0.05 mol/L	100:0
Sa:075	Suberic acid	0.075 mol/L	100:0
Sa:1	Suberic acid	0.1 mol/L	100:0
Asp:005:EG	DL-Aspartic acid	0.005 mol/L	40:60
Asp:025:EG	DL-Aspartic acid	0.025 mol/L	40:60
Asp:05:EG	DL-Aspartic acid	0.05 mol/L	40:60
Asp:075:EG	DL-Aspartic acid	0.075 mol/L	40:60
Asp:1:EG	DL-Aspartic acid	0.1 mol/L	40:60
Sa:005:EG	Suberic acid	0.005 mol/L	40:60

Table 1. *Cont.*

Notation	Organic Additive	Concentration of Additive	Water to Ethylene Glycol Ratio (*v*/*v*)
Sa:025:EG	Suberic acid	0.025 mol/L	40:60
Sa:05:EG	Suberic acid	0.05 mol/L	40:60
Sa:075:EG	Suberic acid	0.075 mol/L	40:60
Sa:1:EG	Suberic acid	0.1 mol/L	40:60

2.2. Characterization

Powder X-ray diffraction data were collected on a Rigaku miniFlex II diffractometer (Rigaku, The Woodlands, TX, USA) working in Bragg–Brentano (θ/2θ) geometry, using Ni-filtered Cu $K\alpha_1$ radiation. The data were collected within a 2θ angle range from 10 to 60° at a step width of 0.01° and speed of 5°/min. Infrared (FTIR) spectra were taken in the range of 4000−400 cm^{-1} with Bruker Alpha ATR spectrometer (Bruker, Billerica, MA, USA). To study the morphological features of the samples, a field-emission scanning electron microscope (FE-SEM), the Hitachi SU-70 (FE-SEM, Hitachi, Tokyo, Japan), was employed.

3. Results

The XRD pattern and FTIR spectrum of starting α-TCP powder used for the synthesis of CDHA are shown in Figures S1 and S2 (see Supplementary Materials), respectively. The XRD pattern did not reveal the presence of neighboring crystalline CP, such as β-TCP or others, and all diffraction peaks were ascribed to α-TCP. The FTIR spectrum confirms the results of XRD analysis. The shape of the spectrum is in a good agreement with those reported in literature [20]; moreover, the absence of absorption band at around 729 cm^{-1} indicates the absence of calcium pyrophosphate, which is a commonly observed impurity in TCP powders synthesized by wet precipitation [21].

In aqueous medium α-TCP reacts with water and converts to calcium-deficient hydroxyapatite ($Ca_9(HPO_4)(PO_4)_5(OH)$, CDHA), as described by the following equation [13]:

$$3\alpha\text{-}Ca_3(PO_4)_2 + H_2O \rightarrow Ca_9(HPO_4)(PO_4)_5(OH) \quad (1)$$

The characteristics of the CDHA sample prepared in aqueous solution under hydrothermal conditions without any additives are given in Figure 1. As seen from the XRD pattern, under selected synthesis conditions α-TCP was fully converted to CDHA, and all diffraction peaks matched the standard XRD data of $Ca_{10}(PO_4)_6(OH)_2$ (ICDD #00-76-0694). There were no peaks associated with the starting material. The SEM image revealed that the morphology of the sample was dominated by plate-like particles of micrometric dimensions. HAp of slightly different morphology was obtained from commercial α-TCP by Goto et al. [13]. The difference might be due to the different starting α-TCP, since the authors used commercial α-TCP of micrometric size, whereas our α-TCP consisted of smaller particles [20].

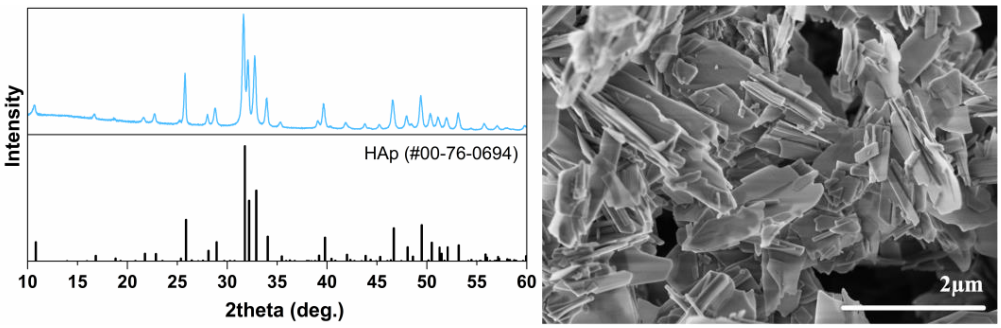

Figure 1. XRD pattern (**left**) and SEM image (**right**) of HAp prepared from α-TCP without additives.

Different results were observed when varying concentrations of SLS and amino acids were applied as additives. The XRD patterns of the final products are given in Figure 2. The lowest concentration of SLS (0.005 mol/L) did not affect the formation of CDHA in terms of phase purity; however, increasing the SLS amount in the reaction solution resulted in the formation of neighboring phase (Figure 2a). In addition to the typical CDHA diffraction pattern, a sharp peak at ca. 25.4° could be seen, and the intensity of this peak gradually increased with an increase in the SLS concentration. This peak was attributed to calcium sulfate ($CaSO_4$, ICDD #00-072-0503). The observed results suggest that under selected synthesis conditions the released Ca^{2+} ions were more easily precipitated by SO_4^{2-} counterions rather than phosphate species. A similar trend was observed for DDDA: the lowest concentration of DDDA (0.005 mol/L) did not affect the formation of CDHA, but higher DDDA content resulted in the formation of secondary crystal phase (Figure 2c). The diffraction peak centered at ca. 13.6° emerged in the XRD pattern of the sample prepared using 0.025 mol/L DDDA. The intensity of this peak increased significantly with an increase in DDDA concentration. This peak corresponded to calcium hydrogen phosphate hydrate (CaH_3O_5P, ICDD #00-046-0494). Hydrothermal reactions in the presence of DL-aspartic and suberic acids resulted in the formation of single-phase CDHA, regardless of the concentration of additives (Figure 2b,d). No formation of impurities or traces of TCP were observed in these cases. It should be noted that in the case of suberic acid (Figure 2d) the intensity of three major peaks varied depending on the concentration of the additive, which could suggest the change in the powders' morphology. To summarize, two of four selected additives led to the formation of secondary phases, while two others did not affect the phase purity.

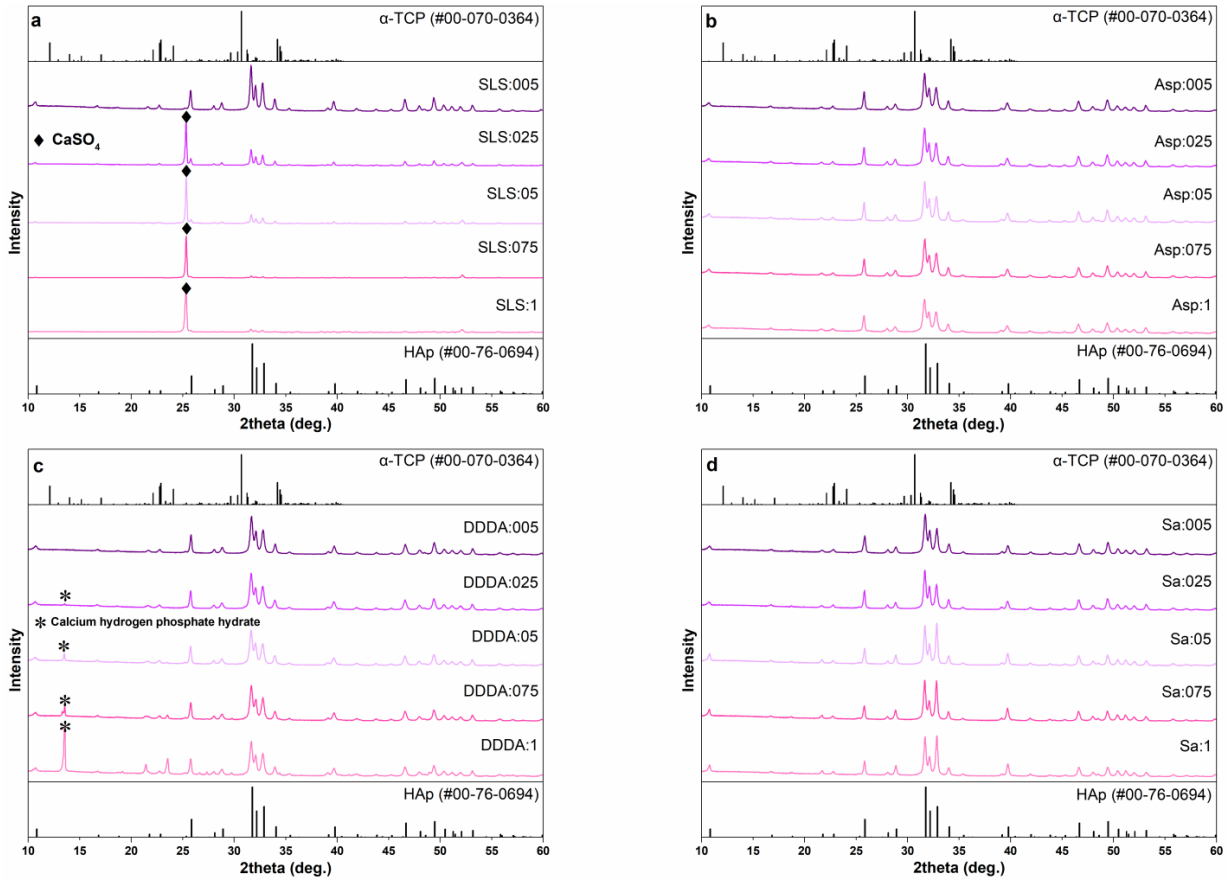

Figure 2. XRD patterns of the samples prepared using various concentrations of SLS (**a**), DL-aspartic acid (**b**), dodecanedioic acid (**c**), and suberic acid (**d**) after a hydrothermal treatment at 200 °C for 5 h.

In this study, we also aimed to check the combined effect of amino acids and organic solvents on the phase purity and morphology of the sample. Since single-phase CDHA was obtained using DL-aspartic and suberic acids, these two additives were used for further experiments. Our previous study revealed that among various organic solvents, ethylene glycol had the greatest influence on the sample morphology [18]. The highest effect on morphology was observed with water to ethylene glycol ratio of 40:60; hence, solvothermal synthesis with DL-aspartic and suberic acids was performed with this mixture. The XRD patterns of the reaction products are demonstrated in Figure 3.

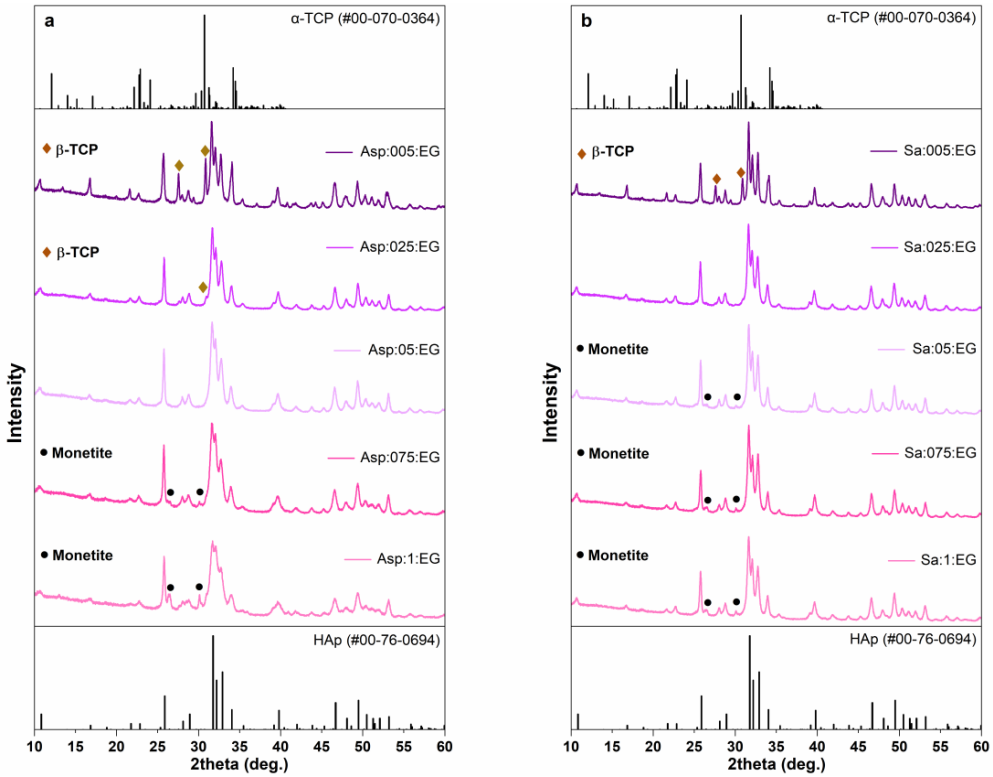

Figure 3. XRD patterns of the samples prepared using various concentrations of DL-aspartic (**a**) and suberic (**b**) acids in water–ethylene glycol mixture (40:60, *v*/*v*) after a solvothermal treatment at 200 °C for 5 h.

It is seen that phase composition strongly depends on the concentration of additive. With the lowest concentration of DL-aspartic acid (0.005 mol/L), a significant amount of neighboring β-TCP phase was obtained along with a major CDHA phase; however, the amount of β-TCP was reduced with an increase in the concentration of additive (Figure 3a). The XRD pattern of the sample synthesized with 0.05 mol/L of aspartic acid did not reveal the presence of any secondary crystal phase. At the same time, the diffraction peaks attributed to monetite ($CaHPO_4$) emerged in the XRD patterns with the highest concentrations of acid (0.075 and 0.1 mol/L). The presence of suberic acid demonstrated a very similar effect (Figure 3b) with a minor difference in phase composition. In this case, a negligible amount of monetite was detected already in the sample with the concentration of acid of 0.05 mol/L. In our previous study [18], the formation of monetite in the presence of organic solvents was also observed at higher temperatures (200 °C) of the solvothermal treatment; however, in this case, increasing concentrations of amino acids promoted the formation of monetite revealing the complex nature of phase transitions in CPs.

Figures 4 and 5 present the FTIR spectra of the samples prepared by hydrothermal and solvothermal treatments.

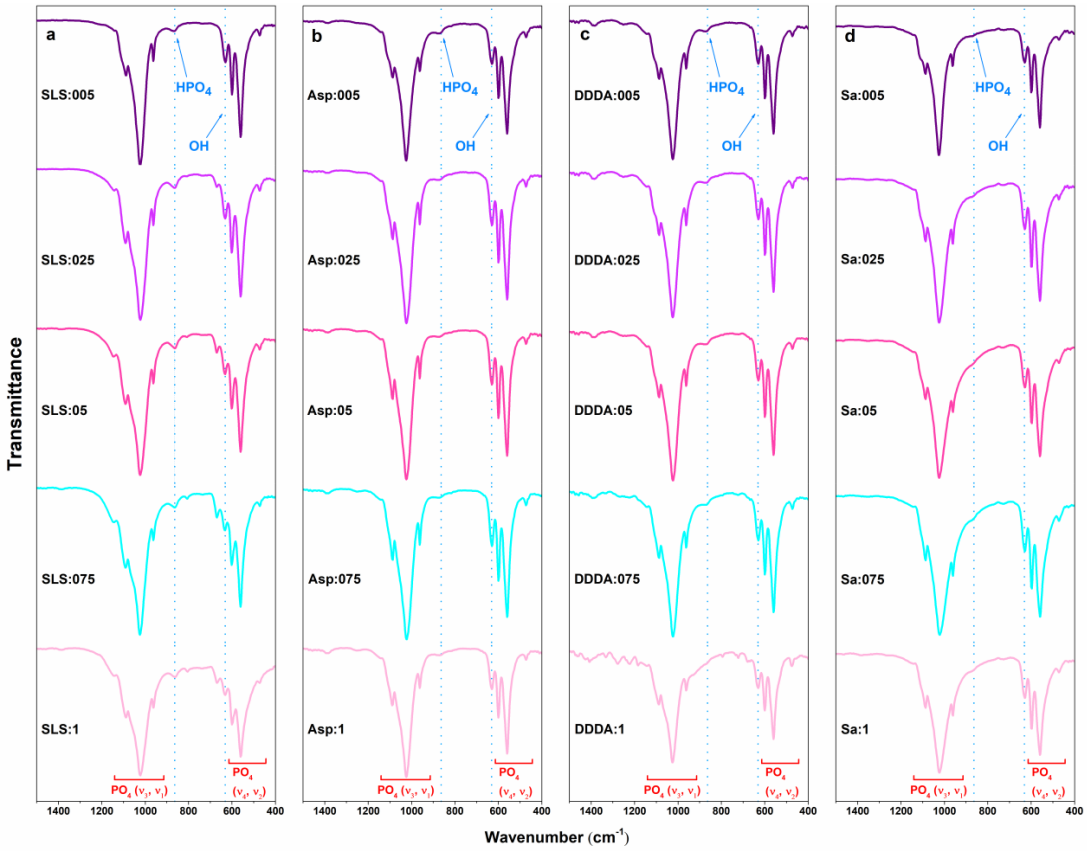

Figure 4. FTIR spectra of the samples prepared using various concentrations of SLS (**a**), DL-aspartic acid (**b**), dodecanedioic acid (**c**), and suberic acid (**d**) after a hydrothermal treatment at 200 °C for 5 h.

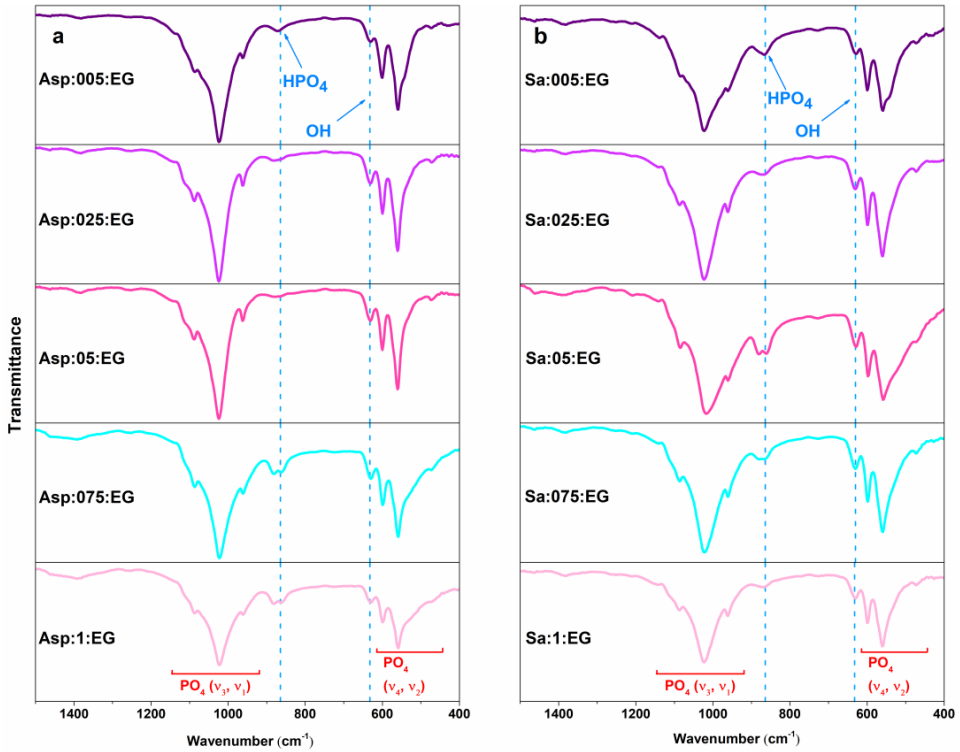

Figure 5. FTIR spectra of the samples prepared using various concentrations of DL-aspartic (**a**) and suberic (**b**) acids in water–ethylene glycol mixture (40:60, v/v) after a solvothermal treatment at 200 °C for 5 h.

The spectral range of 1500–400 cm^{-1} was chosen as representative, because in this range the main absorption bands assigned to CDHA can be observed. As was expected, all the spectra exhibited the absorption bands characteristic of CDHA [22]. The absorption bands of phosphate group in CDHA structure were observed at ca. 560 and 603 cm^{-1} (ν_4), 1020 and 1090 cm^{-1} (ν_3), 960 cm^{-1} (ν_1) which were assigned to O–P–O bending, asymmetric P–O stretching, and symmetric P–O stretching vibrations, respectively. The O–P–O bending vibration mode (ν_2) was observed at 470 cm^{-1} and the band at ca. 630 cm^{-1} was assigned to the hydroxyl group [22]. The absorption band centered at around 870 cm^{-1} was ascribed to the P–O(H) stretching mode of the HPO_4^{2-} group, which confirms the formation of CDHA, since this group is absent in stoichiometric non-deficient HAp [14]. Other bands of low intensity (Figure 4a,c) can be ascribed to the impurities formed during the synthesis and identified by XRD.

The FTIR spectra of synthesized products in the range from 4000 to 400 cm^{-1} are provided in Figures S3–S8; moreover, the spectra of the used organic additives are shown for comparison. The broader range additionally reveals the presence of absorption band centered at ca. 3570 cm^{-1}, which corresponds to the stretching mode of the hydroxyl group [22]. It is seen that in most cases the absorption bands corresponding to additives are absent in the spectra of fabricated CDHA powders, which suggests that the additives were removed from the surface during the washing procedure or the amount of residual organic species is negligible and cannot be detected by FTIR spectroscopy. The only exceptions are the products synthesized with DDDA (Figure S5). The absorption band of DDDA at 1690 cm^{-1} is visible in the spectra of samples synthesized with concentrations of 0.05 mol/L and higher.

The particle size and morphology of HAp are important characteristics of this material due to several reasons [23]. For instance, Dey et al. [24] studied the influence of HAp particle size, morphology, and crystallinity on proliferation of HCT116 colon cancer cells. It was demonstrated that decreasing the HAp powder crystallite size significantly increases the cell inhibition. Another study investigated the effect of nano-HAp particles of different sizes on the proliferation of odontoblast-like MDPC-23 cells comparing them with conventional HAp [25]. The results revealed that nano-HAp expressed an obvious growth-promoting effect. Wen et al. [26] showed that the larger specific surface area associated with the smaller particle size was beneficial for the drug-loading properties of HAp.

The morphology of the samples was found to be dependent both on the nature and concentration of the organic additive. When a small amount of SLS (0.005 mol/L) was used in the hydrothermal reaction, the plate-like crystals dominated in the sample; however, a small number of rods were also seen (Figure 6a). After increasing the amount of organic compound (0.05–0.1 mol/L), the morphology of the CDHA powders changed considerably and rod-shaped assemblies started to form (Figure 6e,i). The huge plate seen in Figure 6i corresponds to $CaSO_4$. The use of low concentration of DL-aspartic acid resulted in the formation of micrometric plate-like particles (Figure 6b), while increasing the amount of acid first led to the reduction of particle size (Figure 6f) and further formation of some rods (Figure 6j). The effect of DDDA was similar to that of aspartic acid and the morphology evolution from plate-like particles to the mixture of plates and rods was observed with an increase in additive concentration. The influence of suberic acid on the morphology of CDHA samples was found to be minor, and plate-like particles were obtained regardless of the concentration of acid. We assume that the effect on the sample morphology might become prominent if the concentrations of suberic acid were further increased.

The SEM images of the samples synthesized in a mixture of water and ethylene glycol in the presence of DL-aspartic and suberic acids are given in Figure 7. In the case of aspartic acid, the presence of the lowest concentration of additive resulted in the formation of a mixture of relatively long rods and short rods (Figure 7a). Using a higher concentration of aspartic acid obtained powders which consisted of micrometric agglomerates, which, in turn, were composed of smaller plate- and rod-like particles (Figure 7b–e). The size of the particles was significantly smaller compared to those synthesized in the aqueous medium

(Figure 6). In the case of suberic acid, relatively large plate-like particles were obtained regardless of the concentration of additive (Figure 7f–j). The morphology was comparable with that of powders obtained by the hydrothermal synthesis with no additives.

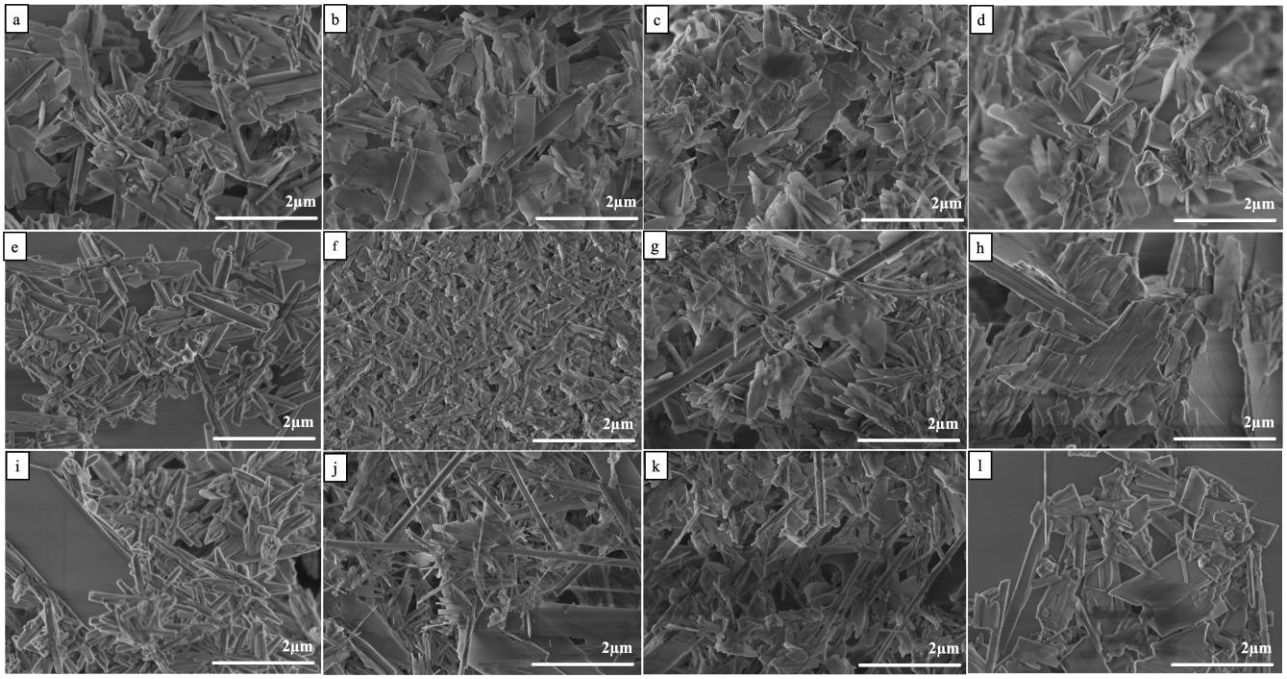

Figure 6. SEM micrographs of the samples after hydrothermal treatment SLS:005 (**a**), SLS:05 (**e**), and SLS:1 (**i**); Asp:005 (**b**), Asp:05 (**f**), and Asp:1 (**j**); DDDA:005 (**c**), DDDA:05 (**g**), and DDDA:1 (**k**); and Sa:005 (**d**), Sa:05 (**h**), and Sa:1 (**l**).

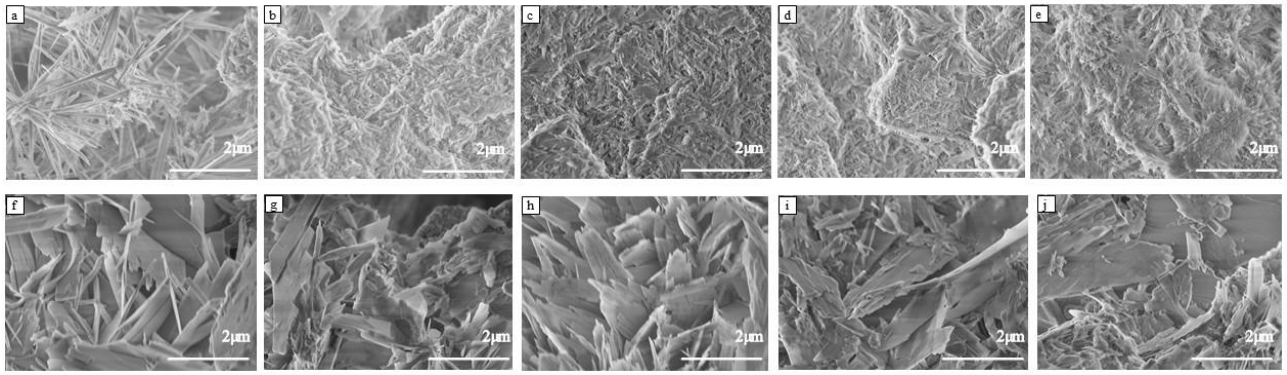

Figure 7. SEM micrographs of the samples after solvothermal treatment under ratio 40:60 of water to ethylene glycol Asp:005:EG (**a**), Asp:025:EG (**b**), Asp:05:EG (**c**), Asp:075:EG (**d**), and Asp:1:EG (**e**); and Sa:005:EG (**f**), Sa:025:EG (**g**), Sa:05:EG (**h**), Sa:075:EG (**i**), and Sa:1:EG (**j**).

To summarize, different impact of additives on the morphology of HAp is probably related to different structures and chemical compositions of organic additives, which leads to a different interaction with HAp particles during the nucleation and crystal growth process.

4. Conclusions

A comprehensive experimental study was carried out to compare the effects of sodium lauryl sulfate and three amino acids (DL-aspartic acid, dodecanedioic acid, and suberic acid) on the formation of calcium-deficient hydroxyapatite via a hydrolysis of α-tricalcium phosphate. It was demonstrated that the phase purity and morphology of the final product strongly depends on the nature and the concentration of organic additives. In aqueous

medium at particular concentrations of sodium lauryl sulfate and dodecanedioic acid, the formation of impurities in addition to hydroxyapatite was observed. On the other hand, the use of aspartic and suberic acids did not affect the phase purity. The different impacts of additives on the morphology of hydroxyapatite are probably related to the different structures and chemical compositions of the organic additives, which lea to different interactions with hydroxyapatite particles during the nucleation and crystal growth process. The morphology of the samples prepared in the aqueous medium varied from plate- to rod-like depending on the concentrations of the specific organic additive. The use of a mixture of water and ethylene glycol led to the formation of significantly smaller particles having a shape of rods and narrow plates.

Supplementary Materials: The following supporting information can be downloaded at: https://www.mdpi.com/article/10.3390/cryst13020265/s1, Figure S1: XRD pattern of α-TCP used for the synthesis of CDHA; Figure S2: FTIR spectrum of α-TCP used for the synthesis of CDHA; and Figures S3–S8: FTIR spectra of the samples prepared using various concentrations of SLS, DL-aspartic acid, dodecanedioic acid, and suberic acid in the range from 4000 to 400 cm^{-1}.

Author Contributions: Conceptualization, R.K., A.Z. and A.K.; methodology, R.K.; validation, E.R.-S., J.-C.Y. and A.I.P.; formal analysis, R.K. and A.I.P.; investigation, R.K., E.R.-S., A.I.P. and J.-C.Y.; resources, A.K.; data curation, A.I.P.; writing—original draft preparation, R.K.; writing—review and editing, A.K.; visualization, R.K.; supervision, A.K.; project administration, A.Z.; and funding acquisition, A.Z. All authors have read and agreed to the published version of the manuscript.

Funding: This research was funded by the grant WHITCERAM (No. S-LJB-22-1) from the Research Council of Lithuania.

Institutional Review Board Statement: Not applicable.

Informed Consent Statement: Not applicable.

Data Availability Statement: Not applicable.

Conflicts of Interest: The authors declare no conflict of interest.

References

1. Habraken, W.; Habibovic, P.; Epple, M.; Bohner, M. Calcium phosphates in biomedical applications: Materials for the future? *Mater. Today* **2016**, *19*, 69–87. [CrossRef]
2. Zikrata, O.V.; Larina, O.V.; Valihura, K.V.; Kyriienko, P.I.; Balakin, D.Y.; Khalakhan, I.; Veltruská, K.; Krajnc, A.; Mali, G.; Soloviev, S.O.; et al. Successive Vapor-Phase Guerbet Condensation of Ethanol and 1-Butanol to 2-Ethyl-1-hexanol over Hydroxyapatite Catalysts in a Flow Reactor. *ACS Sustain. Chem. Eng.* **2021**, *9*, 17289–17300. [CrossRef]
3. Goto, T.; Cho, S.H.; Ohtsuki, C.; Sekino, T. Selective adsorption of dyes on TiO_2-modified hydroxyapatite photocatalysts morphologically controlled by solvothermal synthesis. *J. Environ. Chem. Eng.* **2021**, *9*, 105738. [CrossRef]
4. Ivanets, A.; Zarkov, A.; Prozorovich, V.; Venhlinskaya, E.; Radkevich, A.; Yang, J.-C.; Papynov, E.; Yarusova, S.; Kareiva, A. Effect of Mg^{2+}-, Sr^{2+}-, and Fe^{3+}-substitution on ^{85}Sr and ^{60}Co adsorption on amorphous calcium phosphates: Adsorption performance, selectivity, and mechanism. *J. Environ. Chem. Eng.* **2022**, *10*, 107425. [CrossRef]
5. Sinusaite, L.; Antuzevics, A.; Popov, A.I.; Rogulis, U.; Misevicius, M.; Katelnikovas, A.; Kareiva, A.; Zarkov, A. Synthesis and luminescent properties of Mn-doped alpha-tricalcium phosphate. *Ceram. Int.* **2021**, *47*, 5335–5340. [CrossRef]
6. Zhuang, Z.; Fujimi, T.J.; Nakamura, M.; Konishi, T.; Yoshimura, H.; Aizawa, M. Development of a,b-plane-oriented hydroxyapatite ceramics as models for living bones and their cell adhesion behavior. *Acta Biomater.* **2013**, *9*, 6732–6740. [CrossRef]
7. Kawasaki, T.; Takahashi, S.; Ideda, K. Hydroxyapatite high-performance liquid chromatography: Column performance for proteins. *Eur. J. Biochem.* **1985**, *152*, 361–371. [CrossRef]
8. Kawasaki, T.; Ikeda, K.; Takahashi, S.; Kuboki, Y. Further study of hydroxyapatite high-performance liquid chromatography using both proteins and nucleic acids, and a new technique to increase chromatographic efficiency. *Eur. J. Biochem.* **1986**, *155*, 249–257. [CrossRef]
9. Ezerskyte-Miseviciene, A.; Kareiva, A. Everything old is new again: A reinspection of solid-state method for the fabrication of high quality calcium hydroxyapatite bioceramics. *Mendeleev. Commun.* **2019**, *29*, 273–275. [CrossRef]
10. Bogdanoviciene, I.; Beganskiene, A.; Tõnsuaadu, K.; Glaser, J.; Meyer, H.J.; Kareiva, A. Calcium hydroxyapatite, $Ca_{10}(PO_4)_6(OH)_2$ ceramics prepared by aqueous sol–gel processing. *Mater. Res. Bull.* **2006**, *41*, 1754–1762. [CrossRef]
11. Ferraris, S.; Yamaguchi, S.; Barbani, N.; Cazzola, M.; Cristallini, C.; Miola, M.; Vernè, E.; Spriano, S. Bioactive materials: In vitro investigation of different mechanisms of hydroxyapatite precipitation. *Acta Biomater.* **2020**, *102*, 468–480. [CrossRef] [PubMed]

12. Jung, K.-W.; Lee, S.Y.; Choi, J.-W.; Lee, Y.J. A facile one-pot hydrothermal synthesis of hydroxyapatite/biochar nanocomposites: Adsorption behavior and mechanisms for the removal of copper(II) from aqueous media. *Chem. Eng. J.* **2019**, *369*, 529–541. [CrossRef]
13. Goto, T.; Kim, I.Y.; Kikuta, K.; Ohtsuki, C. Hydroxyapatite formation by solvothermal treatment of α-tricalcium phosphate with water–ethanol solution. *Ceram. Int.* **2012**, *38*, 1003–1010. [CrossRef]
14. Sinusaite, L.; Popov, A.; Raudonyte-Svirbutaviciene, E.; Yang, J.-C.; Kareiva, A.; Zarkov, A. Effect of Mn doping on hydrolysis of low-temperature synthesized metastable alpha-tricalcium phosphate. *Ceram. Int.* **2021**, *47*, 12078–12083. [CrossRef]
15. Suchanek, K.; Bartkowiak, A.; Perzanowski, M.; Marszałek, M. From monetite plate to hydroxyapatite nanofibers by monoethanolamine assisted hydrothermal approach. *Sci. Rep.* **2018**, *8*, 15408. [CrossRef]
16. In, Y.; Amornkitbamrung, U.; Hong, M.-H.; Shin, H. On the Crystallization of Hydroxyapatite under Hydrothermal Conditions: Role of Sebacic Acid as an Additive. *ACS Omega* **2020**, *5*, 27204–27210. [CrossRef]
17. Jiang, S.; Cao, Y.; Li, S.; Pang, Y.; Sun, Z. Dual function of poly(acrylic acid) on controlling amorphous mediated hydroxyapatite crystallization. *J. Cryst. Growth* **2021**, *557*, 125991. [CrossRef]
18. Karalkeviciene, R.; Raudonyte-Svirbutaviciene, E.; Gaidukevic, J.; Zarkov, A.; Kareiva, A. Solvothermal Synthesis of Calcium-Deficient Hydroxyapatite via Hydrolysis of α-Tricalcium Phosphate in Different Aqueous-Organic Media. *Crystals* **2022**, *12*, 253. [CrossRef]
19. Sinusaite, L.; Kareiva, A.; Zarkov, A. Thermally Induced Crystallization and Phase Evolution of Amorphous Calcium Phosphate Substituted with Divalent Cations Having Different Sizes. *Cryst. Growth Des.* **2021**, *21*, 1242–1248. [CrossRef]
20. Sinusaite, L.; Grigoraviciute-Puroniene, I.; Popov, A.; Ishikawa, K.; Kareiva, A.; Zarkov, A. Controllable synthesis of tricalcium phosphate (TCP) polymorphs by wet precipitation: Effect of washing procedure. *Ceram. Int.* **2019**, *45*, 12423–12428. [CrossRef]
21. Torres, P.M.C.; Vieira, S.I.; Cerqueira, A.R.; Pina, S.; da Cruz Silva, O.A.B.; Abrantes, J.C.C.; Ferreira, J.M.F. Effects of Mn-doping on the structure and biological properties of β-tricalcium phosphate. *J. Inorg. Biochem.* **2014**, *136*, 57–66. [CrossRef] [PubMed]
22. Koutsopoulos, S. Synthesis and characterization of hydroxyapatite crystals: A review study on the analytical methods. *J. Biomed. Mater. Res.* **2002**, *62*, 600–612. [CrossRef] [PubMed]
23. Zhou, H.; Lee, J. Nanoscale hydroxyapatite particles for bone tissue engineering. *Acta Biomater.* **2011**, *7*, 2769–2781. [CrossRef] [PubMed]
24. Dey, S.; Das, M.; Balla, V.K. Effect of hydroxyapatite particle size, morphology and crystallinity on proliferation of colon cancer HCT116 cells. *Mater. Sci. Eng. C* **2014**, *39*, 336–339. [CrossRef]
25. Li, N.; Wu, G.; Yao, H.; Tang, R.; Gu, X.; Tu, C. Size effect of nano-hydroxyapatite on proliferation of odontoblast-like MDPC-23 cells. *Dent. Mater. J.* **2019**, *38*, 534–539. [CrossRef]
26. Wen, Y.; Li, J.; Lin, H.; Huang, H.; Song, K.; Duan, K.; Guo, T.; Weng, J. Improvement of Drug-Loading Properties of Hydroxyapatite Particles Using Triethylamine as a Capping Agent: A Novel Approach. *Crystals* **2021**, *11*, 703. [CrossRef]